INTERNATIONAL JOURNAL FOR NUMERICAL METHODS IN FLUIDS
Int. J. Numer. Meth. Fluids 2001; **37**: 577–600 (DOI: 10.1002/fld.188)

Solving free surface fluid flow problems by the minimal kinetic energy functional

J. K. Lonyangapuo[a], L. Elliott[a,*,1], D. B. Ingham[a] and X. Wen[b]

[a] *Department of Applied Mathematics, University of Leeds, Leeds, U.K.*
[b] *Environment Centre, University of Leeds, Leeds, U.K.*

SUMMARY

In this paper a more accurate minimization technique, namely the minimal kinetic energy method, is developed and used to investigate the free surface fluid flow caused by an obstacle on the bottom of a channel whose exact shape and location are unknown *a priori*. The fluid flow is assumed to be two-dimensional, steady, inviscid, incompressible, irrotational and under the effect of the gravitational force. The minimization technique is based on the combination of the boundary integral method and the variational principle technique. This technique is extensively used in identifying unknown bottom surfaces. To illustrate this technique the free surface profile to be applied in the inverse analysis has been generated following a direct formulation when the solid bottom boundary possesses a double hump/double depression, a hump in front of a step, and a depression and a hump in front of a step. For all problems considered, the numerical results are in excellent agreement with the known analytical solution. In fact the computed profiles for both the bottom and free surfaces are graphically indistinguishable from the analytical results. Copyright © 2001 John Wiley & Sons, Ltd.

KEY WORDS: boundary integral method; free surface flows; minimal functional; minimal kinetic energy method; minimization technique; variational principle technique

1. INTRODUCTION

The free surface flow of a two-dimensional, steady, incompressible, irrotational and inviscid fluid under the influence of gravity has been the subject of considerable research in hydraulic engineering and coastal engineering over several decades. Some examples where free surface flows are encountered are in the seepage of ground water, free jets, flows over ramps, sluice gates, stratified flows, melting of ice, gravity waves, etc. An increasing demand for the utilization of the resources of free surface fluid flow problems has forced mathematicians, physicists and engineers to develop many of the necessary computational tools and techniques with which to study such situations. In fact research interest in studies started as early as the

* Correspondence to: School of Mathematics, University of Leeds, Leeds, LS2 9JT, U.K.
[1] E-mail: amt6dbi@amsta.leeds.ac.uk

Received July 2000
Revised November 2000

1940s and since then it has developed in two main areas, namely the direct and indirect approaches. The terms direct and indirect approaches are taken to mean the investigation of the free surface fluid flow when the bottom surface is known *a priori* but the free surface is not known, and when the free surface is given but the bottom surface is unknown *a priori*, respectively.

Many of the previous investigations into free surface fluid flow problems have used a direct approach, and there are numerous publications in the literature. Both numerical space discretization and boundary element methods have been used to determine the free surface fluid flows over complex geometries in numerous hydraulic engineering research areas. Forbes and Schwartz [1] used the boundary element method (BEM) to formulate the governing boundary integral equations for free surface flows over a semi-circular step in a channel. Boutrous and El-Malek [2] used the Hilbert method to solve numerically the uniform channel fluid flow over irregular bottom topographies, and King and Bloor [3] have examined the steady, two-dimensional fluid flow over an arbitrary bed topography using a conformal mapping technique based on a generalized Schwarz–Christoffel transformation.

More recently, Wen and Wu [4] and Wen and Ingham [5] have developed a technique which combines the use of the boundary integral method (BIM), the Riemann–Hilbert method and Muskhelishvili's singular integral equation theory [6], so that the resulting non-linear boundary integral equations that are formed may be solved numerically. Boundary integral equations are derived in which the non-dimensional distance s along the streamlines is taken as an independent variable and the non-dimensional velocity potential ϕ on the solid boundary and the free surface boundary are the dependent variables. Thus, in the integral equation, the geometry of the solid boundary is no longer an unknown function. An iterative method for solving the integral equations is suggested in order to obtain gravity affected fluid flows over a curved boundary with a free surface. This method has been applied to the free surface flow past a spillway by Wen and Wu [4], to three-layer stratified fluid flows by Wen and Ingham [5], to the investigation of the free surface fluid flow over a step of a constant slope/arbitrary shape in a channel by Wen *et al.* [7,8], and to the critical height in a channel for a wave-free potential free surface flow by Lonyangapuo *et al.* [9].

However, in many free surface problems that are currently of interest, the free surface position and the fluid speed on this boundary are given but the shape and location of the solid bottom boundary and the fluid speed on this boundary are unknown *a priori*. These free surface problems are called indirect problems for which we have found no previous publications in the literature. Research activities on inverse free surface fluid flow problems failed initially because the available techniques could not handle the highly ill-posed problems being formulated and the associated non-linear integral equations. However, powerful computers are now available which can handle large mathematical and computational problems that are normally associated with indirect problems. Over the last 3 years we have performed a considerable amount of research in this field and have established important minimization techniques to solve these problems. The aim of this paper is to present a more accurate minimization technique to solve free surface fluid flows over obstacles of unknown shape and location. This new technique is the minimization of the total kinetic energy.

Lonyangapuo *et al.* [10,11] have developed a minimization technique in order to solve such problems. This approach was based upon the minimization of the sum of the squares of the

distances between the simulated free surface position from the direct problem and the computed value determined by the direct formulation from the estimated solid bottom surface position. An iterative technique ensured that for monotonically increasing geometries of the lower surface the inverse procedure could accurately recover this shape using only the known position of the free surface. However, the failure of the minimization procedure to incorporate any physical features meant that only the simplest of geometries could be successfully recovered. More significant progress on the investigation of the inverse free surface flows was reported by Lonyangapuo *et al.* [12–14]. In these papers, two physical aspects of the problem, namely the total fluid pressure and total fluid energy, were taken into consideration. These two physical aspects were formulated as extremum functionals, namely the extremum total pressure and the extremum energy functionals and presented as possible candidates for the minimization problem. However, since these functionals were not formulated on rigorous physical arguments, it means that the nature of their extrema is somewhat unclear and highly dependent on the chosen functionals themselves, making it necessary to investigate the occurrence of both types of extrema. The determination of the extrema of both the total pressure and the total energy were developed and used to identify the bottom surface which may not necessarily be represented by a monotonically increasing function, as was the situation investigated by Lonyangapuo *et al.* [10,11].

Lonyangapuo *et al.* [12–14] found that for free surfaces corresponding to fluid flow over monotonically decreasing or increasing bottom surfaces, both the minimization and maximization of the pressure and energy functionals were capable of retrieving the geometrical shape of the lower boundary. In addition, for free surfaces corresponding to flow over single humps and single depressions, the obstacle could be retrieved by taking the minimization and the maximization of the respective functionals. However, regardless of the type of extrema, these techniques were unable to solve more complex problems, since they failed when the solid bottom surface was a double hump or a double depression. Although the results were optimal, the predicted bottom surfaces were not in agreement with the analytical ones and therefore these methods still fell short of what is required to identify complex geometrical bottom surfaces using a consistent sign formulation. In this paper we apply the minimal kinetic energy functional in identifying the bottom surface when it possesses a double hump/depression, a hump in front of a step, and both a depression and a hump in front of a step.

In all the previous techniques we have been comparing the computed solution with the analytical solution, since we have no *prior* information about the nature of the functional to be minimized. To prove that the minimal kinetic energy technique is robust enough we extend this technique to free surface fluid flow problems whose free surface position is arbitrarily given but the analytical bottom solid boundary is not known. As an example of such a situation we investigate the existence of the bottom surface when the free surface profile is given by the function $y = \tanh(x)$.

2. PROBLEM FORMULATION

In this paper we concentrate on investigating inverse free surface fluid problems caused by more complex geometrical bottom surfaces of a channel which could not be solved by the

previous techniques, see Lonyangapuo *et al.* [11–14]. However, first it is worthwhile stating that the minimal kinetic energy functional has been applied to the simple problems considered in these papers and extremely good results obtained; hence they are not repeated here. These problems are caused by the fluid flow over a step, a fall, a hump and a depression, and for their formulations, see Lonyangapuo *et al.* [14].

First, we consider the case when a double hump and a double depression occur on the bottom surface of a channel. Far upstream of the double hump/depression the fluid is of dimensional depth h and flows horizontally in the positive X direction with a uniform dimensional speed of magnitude U_∞. The upstream and downstream infinity positions are denoted by X_E and X_F respectively, and the double hump/depression, together with the maximum height/depth, is assumed to be located in the region $X_1 \leq X \leq X_2$. The shape of the bottom surface is initially assumed to be governed by the function $Y_b = f(X)$ and the angle the solid bottom surface makes with the horizontal is given by $\beta(X) = \tan^{-1}(f'(X))$. For $X \geq X_F$, the fluid flow is assumed to be uniform and the dimensional fluid depth again reaches h (Figure 1(a) and (b)). On the bottom of the channel, the dimensional streamfunction Ψ is chosen, without any loss of generality, such that $\Psi = 0$, and therefore on the free surface we can take $\Psi = Q^* = U_\infty h$. The third and fourth problems we have investigated are when there is a hump in front of a step and when both a depression and a hump are in front of a step, and all these shapes occur on the bottom surface of a channel. The obstacles are assumed to be located in the region, $X_1 \leq X \leq X_2$ and the maximum dimensional height reached by these obstacles occurs in this region (Figure 1(c) and (d)).

A rectangular co-ordinate system $Z = X + \mathrm{i}\,Y$ is introduced such that the X-axis is horizontal and the Y-axis is vertically upwards. This assumption allows the introduction of a dimensional velocity potential Φ and a dimensional streamfunction Ψ such that the dimensional velocity potential $W = \Phi + \mathrm{i}\Psi$ is an analytic function in the domain occupied by the fluid. Bernoulli's equation at any point in the fluid flow in the channel is given by

$$\frac{P_\infty}{\rho g h} + \frac{U_\infty^2}{2gh} + 1 = \frac{P}{\rho g h} + \frac{U^2}{2gh} + \frac{Y}{h} \tag{1}$$

where U_∞ is the dimensional velocity far upstream, P_∞ is the dimensional atmospheric pressure, ρ is the fluid density, g is the magnitude of the gravitational acceleration, U and P are the dimensional velocity and dimensional pressure, respectively, at any general point in the fluid flow.

At the free surface, on which $P = P_\infty$, Equation (1) gives the free surface non-dimensional fluid velocity, namely

$$u_f = \frac{U_f}{U_\infty} = \sqrt{\left[1 + \frac{2}{Fr^2}(1 - y_f)\right]} \tag{2}$$

where $y_f = Y_f/h$ is the non-dimensional free surface height and $Fr = U_\infty/\sqrt{gh}$ is the upstream Froude number. Equation (2) can also be written in the form

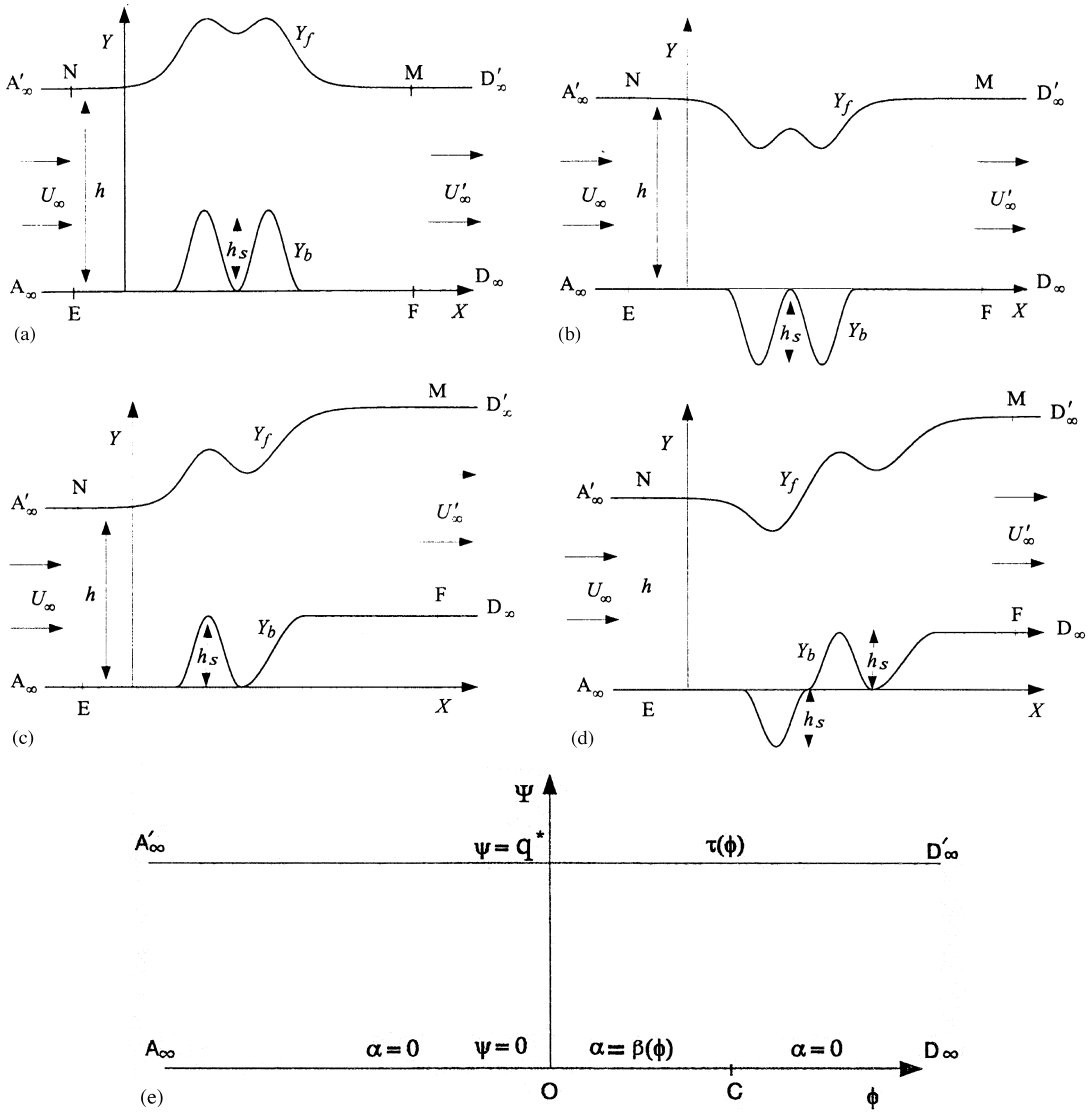

Figure 1. (a), (b), (c) and (d) show a schematic diagram of the physical problems and the notation employed, while (e) and (f) show the infinite plane and the upper half plane, respectively.

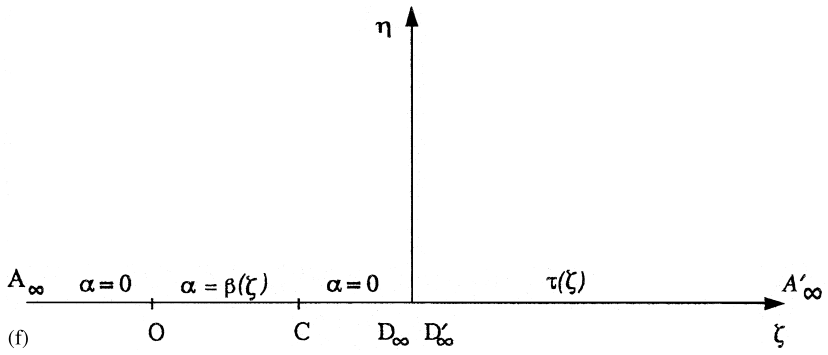

Figure 1 (*Continued*)

$$\ln(u_f) = \ln\left(\sqrt{\left[1 + \frac{2}{Fr^2}(1 - y_f)\right]}\right) = \tau_f \tag{3}$$

where the parameter τ_f plays a significant part in the formulation of the expression for θ, the angle that the fluid velocity vector on the free surface makes with the horizontal.

We next consider the complex velocity which is expressed as

$$\frac{dW}{dZ} = U\, e^{-i\alpha} \tag{4}$$

where α and U are the angle the fluid velocity vector makes with the positive X-axis and the dimensional fluid velocity at any point in the flow field respectively. On the bottom and the free surface, α becomes β and θ respectively. Then the logarithm of the complex fluid velocity is given by

$$\Omega = \ln\left(\frac{1}{U_\infty}\frac{dW}{dZ}\right) = \tau - i\alpha \tag{5}$$

where $\tau = \ln(U/U_\infty)$, and τ, dW/dZ and Ω are analytical functions in an infinite strip of the flow field (Figure 1(e)). This infinite strip is transformed onto the upper half plane of the auxiliary plane by applying a conformal mapping function derived by use of the Schwarz–Christoffel transformation (Figure 1(f)). Equation (5) is in the form of a Riemann–Hilbert problem whose solution is obtained by using the Riemann–Hilbert method, with $\tau = \tau_b = \ln(U_b/U_\infty)$ and $\alpha = \theta$ being unknown quantities on the bottom surface and the free surface respectively. In this paper the following transformations $x = X/h$, $y = Y/h$, $u = U/U_\infty$, $p = P/\rho U_\infty^2$ and $w = W/U_\infty$, are applied. Other non-dimensional quantities obtained following this transformation are as follows: $x_1 = X_1/h$, $x_2 = X_2/h$, $y = Y/h$, $x_E = X_E/h$, $x_F = X_F/h$, $x_b = X_b/h$, $x_f = X_f/h$, $y_b = Y_b/h$, $y_f = Y_f/h$, $u_b = U_b/U_\infty$, $\psi = \Psi/U_\infty h$ and $\phi = \Phi/U_\infty h$.

For the four problems the equation governing the fluid motion is the Laplace equation, see for example Lamb [15], and can be written as follows:

$$\frac{\partial^2\phi}{\partial x^2}+\frac{\partial^2\phi}{\partial y^2}=0; \quad -\infty<x<\infty, \quad y_b\le y<y_f \tag{6}$$

where y_b and y_f are the non-dimensional bottom and free surfaced heights respectively. This equation is solved subject to the boundary condition $\partial\phi/\partial n=0$, where n is an outward normal to the free surface and the bottom surface boundaries. In addition, $\partial\phi/\partial x$ is specified at large non-dimensional distances both upstream and downstream, i.e. at x_E and $x_{F.}$

Thus the non-dimensional conformal mapping function employed for the infinite strip-half plane transformation, which is derived by use of the Schwarz–Christoffel transformation, may be written in the form

$$t=-e^{-((\pi/q^*)w)} \tag{7}$$

where $q^*=Q^*/U_\infty h=1$. When $t=\zeta+i\eta$ and $w=\phi+i\psi$ are substituted into Equation (7), we obtain

$$\zeta+i\eta=-e^{-\pi(\phi+i\psi)} \tag{8}$$

The bottom solid and free surface boundaries in the physical plane now lie in the real axis, ζ, of the upper half plane. At this stage, the usual steps for solving the Riemann–Hilbert boundary problem for the half plane are followed, see for example Wen *et al.* [8] and Lonyangapuo *et al.* [14]. At any point $\zeta=\zeta_0$, the real part $\tau(\zeta_0)$ for the present Riemann–Hilbert boundary problem defines the logarithm of the fluid speed on the bottom surface and may be expressed as follows:

$$\tau(\zeta_0)=\frac{\sqrt{-\zeta_0}}{\pi}\left[\oint_{-\infty}^{0}\frac{-\beta(\zeta)}{\sqrt{-\zeta}(\zeta-\zeta_0)}\,d\zeta+\int_0^\infty\frac{\tau(\zeta)}{\sqrt{\zeta}(\zeta-\zeta_0)}\,d\zeta\right], \quad \zeta<0 \tag{9}$$

whereas the imaginary part, $\Omega(\zeta_0)$, which is the angle the fluid velocity vector on the free surface makes with the positive x-axis, is given by

$$\theta(\zeta_0)=\frac{\sqrt{\zeta_0}}{\pi}\left[\int_{-\infty}^{0}\frac{-\beta(\zeta)}{\sqrt{-\zeta}(\zeta-\zeta_0)}\,d\zeta+\int_0^\infty\frac{\tau(\zeta)}{\sqrt{\zeta}(\zeta-\zeta_0)}\,d\zeta\right], \quad \zeta<0 \tag{10}$$

Since the independent variable used in this paper is the non-dimensional height of the solid surface, y_b, the angle that the bottom solid boundary makes with the horizontal can be obtained numerically but in this paper we have used finite difference as follows:

$$\beta_i=\frac{y_{b(i+1)}-y_{b(i-1)}}{x_{b(i+1)}-x_{b(i-1)}}, \quad \text{for } i=1,2,\ldots,m \tag{11}$$

where $(x_b(i), y_b(i))$ is the non-dimensional co-ordinate of a general point on the solid bottom surface.

The values of x_b, the known free surface position (x_f^k, y_f^k) and the non-dimensional fluid speed on the free surface boundary u_f^k are all known *a priori*. The superscript k denotes known quantities on the free surface. At this point, we introduce s to represent the non-dimensional arc length along both the free surface and bottom surface boundaries. On the bottom of the channel we have the following relation:

$$\frac{d\phi_b}{ds} = u_b(s) \tag{12}$$

which on integration yields

$$\phi_b(s) = \phi_E + \int_0^s u_b(l)\, dl \tag{13}$$

where ϕ_b is the non-dimensional potential function along the bottom surface and ϕ_E is the value of the non-dimensional potential function at the point E. Similarly, the non-dimensional potential function, ϕ_f, on the free surface may be found as follows:

$$\frac{d\phi_f}{ds} = u_f^k(s) \tag{14}$$

which on integration yields

$$\phi_f^k(s) = \phi_N + \int_0^s u_f^k(l)\, dl \tag{15}$$

where ϕ_f^k is the non-dimensional potential function along the free surface and it is a known quantity since u_j^k is known *a priori*. We shall also make use of the following identities:

$$\frac{dx}{ds} = \cos\alpha \tag{16}$$

$$\frac{dy}{ds} = \sin\alpha \tag{17}$$

where on the free surface and the bottom surface boundaries, α assumes the values θ and β respectively. On integrating Equations (16) and (17), we obtain the expressions for the computed non-dimensional co-ordinates of the free surface as follows:

$$x_f^c(s) = x_N + \int_0^s \cos\theta(l)\, dl \tag{18}$$

$$y_{\mathrm{f}}^{\mathrm{c}}(s) = y_N + \int_0^s \sin\theta(l)\,\mathrm{d}l \tag{19}$$

where x_N and y_N are the non-dimensional co-ordinates of the point N. The superscript c appearing in the co-ordinate $(y_{\mathrm{f}}^{\mathrm{c}}, y_{\mathrm{f}}^{\mathrm{c}})$ has been used in order to differentiate it from that of the known free surface co-ordinate $(y_{\mathrm{f}}^{\mathrm{k}}, y_{\mathrm{f}}^{\mathrm{k}})$, where k denotes known.

On using Equation (8) in Equations (9) and (10), we obtain the equations for $\tau(s)$ and $\theta(s)$ in the physical plane as follows:

$$\begin{aligned}\tau_{\mathrm{b}}(s) &= \ln(u_{\mathrm{b}}(s)) \\ &= \sqrt{\mathrm{e}^{-\pi\phi(s)}}\left[\int_{\Gamma_1} \frac{\beta(l)}{\sqrt{\mathrm{e}^{-\pi\phi(l)}}(-\mathrm{e}^{\pi\phi(l)} + \mathrm{e}^{-\pi\phi(s)})}\,\mathrm{e}^{-\pi\phi(l)}u(l)\,\mathrm{d}l\right. \\ &\quad \left. - \int_{\Gamma_2} \frac{\tau_{\mathrm{f}}(l)}{\sqrt{\mathrm{e}^{-\pi\phi(l)}}(\mathrm{e}^{-\pi\phi(l)} - \mathrm{e}^{-\pi\phi(s)})}\,\mathrm{e}^{-\pi\phi(l)}u(l)\,\mathrm{d}l\right], \quad s\in\Gamma_1\end{aligned} \tag{20}$$

$$\begin{aligned}\theta^{\mathrm{c}}(s) &= \frac{\sqrt{\mathrm{e}^{-\pi\phi(s)}}}{q}\left[\int_{\Gamma_1} \frac{\beta(l)}{\sqrt{\mathrm{e}^{-\pi\phi(l)}}(-\mathrm{e}^{-\pi\phi(l)} + \mathrm{e}^{-\pi\phi(s)})}\,\mathrm{e}^{-\pi\phi(l)}u(l)\,\mathrm{d}l\right. \\ &\quad \left. - \int_{\Gamma_2} \frac{\tau_{\mathrm{f}}(l)}{\sqrt{\mathrm{e}^{-\pi\phi(l)}}(\mathrm{e}^{-\pi\phi(l)} - \mathrm{e}^{-\pi\phi(s)})}\,\mathrm{e}^{-\pi\phi(l)}u(l)\,\mathrm{d}l\right], \quad s\in\Gamma_2\end{aligned} \tag{21}$$

where $\tau_{\mathrm{f}}(l)$ is determined from expression (3).

The set of equations (13) and (18)–(21) are the boundary integral equations for the non-dimensional potential function on the bottom solid boundary, $\phi_{\mathrm{b}}(s)$, the non-dimensional computed co-ordinates of the free surface, $x_{\mathrm{f}}^{\mathrm{c}}(s)$ and $y_{\mathrm{f}}^{\mathrm{c}}(s)$, the non-dimensional fluid speed on the bottom solid bottom boundary, $u_{\mathrm{b}}(s)$, and the angle that the computed free surface makes with the horizontal, $\theta^{\mathrm{c}}(s)$. Since $y_{\mathrm{f}}^{\mathrm{k}}(s)$ is known, then $\theta^{\mathrm{k}}(s)$, $\tau_{\mathrm{f}}(s)$, $u_{\mathrm{f}}(s)$ and $\phi_{\mathrm{f}}(s)$ are also known, so that the unknowns in Equations (20) and (21) are $\beta(s)$, $\phi_{\mathrm{b}}(s)$ and $u_{\mathrm{b}}(s)$.

The numerical integration of the set of equations (13) and (18)–(21) over each interval is calculated by use of the mean value theorem for integrals, such that over each interval $[i, i+1]$ we take $\beta(l) = (\beta_i + \beta_i + 1)/2$ and $\tau(l) = (\tau_i + \tau_i + 1)/2$. For the complete numerical integration and the resulting equations, see Lonyangapuo *et al.* [14].

2.1. The minimal kinetic energy method

If a mass of fluid is set in motion by giving prescribed velocities to its boundaries then the kinetic energy generated in the actual fluid motion is less than that of any other possible motion consistent with the same motion of the boundaries. This important theorem is due to Lord Kelvin, see Ramsey [16]. Therefore, we propose the minimal kinetic energy functional as the minimization technique, and it is derived from Green's Theorem as follows:

$$\frac{\rho}{2}\iiint_V \left[\left(\frac{\partial\phi}{\partial x}\right)^2 + \left(\frac{\partial\phi}{\partial z}\right)^2 + \left(\frac{\partial\phi}{\partial z}\right)^2\right]\mathrm{d}x\,\mathrm{d}y\,\mathrm{d}z = \frac{\rho}{2}\oint_s \phi\,\frac{\partial\phi}{\partial n}\,\mathrm{d}S \tag{22}$$

where x, y, z are independent variables, ϕ is the dependent variable, ρ is the fluid density and S is a surface enclosing volume V of the fluid. Let F^* denote the kinetic energy functional, then Equation (22) can be written as

$$F^* = \frac{\rho}{2} \oint_s \phi \frac{\partial \phi}{\partial n} \, \mathrm{d}S \tag{23}$$

On expanding Equation (23) along the fluid boundaries for our two-dimensional free surface fluid flow over an unknown lower boundary (Figure 1(a)–(d)), we find F^* in terms of the integral of ϕ times the fluid velocity over the total surface on all the boundaries, i.e.

$$F^* = \frac{\rho}{2} \int_{\mathrm{in}} \phi \frac{\partial \phi}{\partial n} \, \mathrm{d}y + \frac{\rho}{2} \int_{\mathrm{bot}} \phi \frac{\partial \phi}{\partial n} \, \mathrm{d}S + \frac{\rho}{2} \int_{\mathrm{fre}} \phi \frac{\partial \phi}{\partial n} \, \mathrm{d}S + \frac{\rho}{2} \int_{\mathrm{out}} \phi \frac{\partial \phi}{\partial n} \, \mathrm{d}y \tag{24}$$

where the notations, in, fre, bot and out are used to show the integration across the upstream inlet, the free surface, the bottom surface and the downstream outlet, respectively. As on both the free and the bottom surfaces the fluid does not penetrate the boundary, i.e. $\partial \phi / \partial n = 0$, Equation (24) reduces to

$$F^* = \frac{\rho}{2} \int_{\mathrm{in}} \phi \frac{\partial \phi}{\partial n} \, \mathrm{d}y + \frac{\rho}{2} \int_{\mathrm{out}} \phi \frac{\partial \phi}{\partial n} \, \mathrm{d}y \tag{25}$$

In addition, far upstream and downstream $\partial \phi / \partial n$ becomes $-\partial \phi / \partial x$ and $\partial \phi / \partial x$ respectively. The integral for the inlet flow can be omitted since both the values of ϕ and $\partial \phi / \partial n$ are known constants at the inlet. Therefore, Equation (25) finally takes the form

$$F = \int_{\mathrm{out}} \phi \frac{\partial \phi}{\partial x} \, \mathrm{d}y \tag{26}$$

where F is the modified functional and the constant $\rho/2$ is omitted since it does not affect the position of the required minimum. Thus, Equation (26) is the final form of the kinetic energy functional in a two-dimensional, steady, inviscid, incompressible and irrotational fluid flow.

Unlike the previous two minimization techniques, namely the total pressure and the total energy functionals, see Lonyangapuo *et al.* [14], the minimal kinetic energy can be shown to lead to the Laplace equation. This can be demonstrated by applying the variational technique to Equation (26). Since Equation (26) is a modified form of Equation (22), applying the variational technique to both equations lead to the same result. Therefore we shall use the left-hand side of Equation (20) to show that the minimal kinetic energy functional leads to the Laplace equation. This is done with the help of the Euler–Lagrange equation in the form

$$\frac{\partial Q}{\partial \phi} - \frac{\partial}{\partial x} \frac{\partial Q}{\partial \phi_x} - \frac{\partial}{\partial y} \frac{\partial Q}{\partial \phi_y} - \frac{\partial}{\partial z} \frac{\partial Q}{\partial \phi_z} = 0 \tag{27}$$

where $Q = Q(\phi, \phi_x, \phi_y, \phi_z, x, y, z)$ is an integrand of the integral equation

$$I = \iiint_V Q\left(\phi, \frac{\partial\phi}{\partial x}, \frac{\partial\phi}{\partial y}, \frac{\partial\phi}{\partial z}, x, y, z\right) \mathrm{d}x\ \mathrm{d}y\ \mathrm{d}z \tag{28}$$

It is seen that the minimal kinetic energy functional, as given by the left-hand side of Equation (22), is in the form of Equation (28) where

$$Q = \frac{\rho}{2}[\phi_x^2 + \phi_y^2 + \phi_z^2] \tag{29}$$

and $\phi_x = \partial\phi/\partial x$, etc.

On substituting Q from Equation (29) into the Euler–Lagrange Equation (27), we have

$$\frac{\rho}{2}\frac{\partial[\phi_x^2 + \phi_y^2 + \phi_z^2]}{\partial\phi} - \frac{\rho}{2}\frac{\partial}{\partial x}\frac{\partial[\phi_x^2 + \phi_y^2 + \phi_z^2]}{\partial\phi_x} - \frac{\rho}{2}\frac{\partial}{\partial y}\frac{\partial[\phi_x^2 + \phi_y^2 + \phi_z^2]}{\partial\phi_y} - \frac{\rho}{2}\frac{\partial}{\partial z}\frac{\partial[\phi_x^2 + \phi_y^2 + \phi_z^2]}{\partial\phi_z} = 0 \tag{30}$$

and simplification of this equation leads to

$$[\phi_{xx} + \phi_{yy} + \phi_{zz}] = 0 \tag{31}$$

where $\phi_{xx} = \partial^2\phi/\partial x^2$, etc. However, in this paper we have taken the fluid flow to be two-dimensional and hence equation (31) reduces to

$$\phi_{xx} + \phi_{yy} = 0 \tag{32}$$

or

$$\nabla^2\phi = 0 \tag{33}$$

which is the required Laplace equation for a two-dimensional fluid flow.

We now use a minimization method which is based on the sequential quadratic programming (SQP) algorithm, which minimizes any smooth non-linear functional subject to a set of pre-assigned constraints on the independent variables, y_b, and a set of non-linear constraints. For a detailed discussion on the SQP method, see the NAG routine E04UCF and Gill *et al.* [17]. The parameters $y_b^{\min}$, $y_b^{\max}$, Fr, ϵ_1 and ϵ_2 play a significant role in the solution technique for this problem, where $y_b^{\min}$ and $y_b^{\max}$ are the lower and upper bounds on the independent variables y_b, respectively, and ϵ_1 and ϵ_2 are accuracy parameters. The minimal kinetic energy method is obtained from the kinetic energy functional, see Equation (26), in the form

$$\min_{\underline{y}_b \in R^m} F(\underline{y}_b) = \phi_{bm} \times u_{bm} \times [y_{fm}^k - y_{bm}] \tag{34}$$

where F is a non-linear functional, $x_{bm} = x_F$ is the x-value at the downstream infinity position,

m is the total number of grid points used, (x_F, y_{bm}) is the position of the non-dimensional bottom surface at $x_{bm} = x_F$, (x_F, y^k_{fm}) is the position of the non-dimensional free surface at $x_{fm} = x_F$, ϕ_{bm} and u_{bm} are the values of the non-dimensional velocity potential and the non-dimensional fluid velocity, respectively, on the bottom surface at the far downstream infinity position. The simple constraints on y_b are given by

$$y_b^{\min} \le y_{bi} \le y_b^{\max}; \qquad x_E \le x_{bi} \le x_F \quad i = 1, 2, \ldots, m \tag{35}$$

while the non-linear constraints are defined as

$$(y^k_{fj} - \epsilon_1) \le y^c_{fj} \le (y^k_{fj} + \epsilon_2), \quad j = 1, 2, \ldots, n \tag{36}$$

where, as mentioned earlier, ϵ_1 and ϵ_2, y^k_{fj} and y^c_{fj} are accuracy parameters, the computed and the given non-dimensional free surface heights, respectively. The parameter n denotes the total number of non-linear constraints used, where $n \le m$. In this paper we have taken the number of non-linear constraints to be $n = m/2$. Equations (34)–(36) define the new minimization technique which we apply in the investigation of the inverse free surface fluid flow problems.

In all the problems investigated in this paper using the minimal kinetic energy functional, while the value of ϵ_2 is fixed at zero, the value of ϵ_1 is allowed to vary until a particular small value is identified that corresponds to when there is no feasible solution to the non-linear constraints. Setting $\epsilon_2 = 0$ means that y^c_f is not allowed to be greater than y^k_f and for the present problems we found that the best values of ϵ_1 lie in the range $10^{-4} \le \epsilon_1 \le 10^{-3}$. The constrained minimization problem (34)–(36) is solved numerically using the NAG routine E04UCF until an optimum solution, denoted by y_b^{opt}, is obtained or until a local minimum is attained and no further improvement can be made.

The choice of the initial estimate for the non-dimensional height of the bottom surface, h_b^{int}, is not crucial in these problems as to whether or not a solution may be obtained which is in the feasible region. In this investigation we start with a very approximate guess for the initial estimate of the location of the bottom surface and then find by the direct approach the corresponding initial non-dimensional height of the free surface, y_f^{int}. Then by choosing the first predicted solution as the next initial estimate, with ϵ_1 taking a smaller value than that used for the first approximation, we can progressively improve on the predicted solution until an optimal solution, y_b^{opt}, is attained. This solution y_b^{opt} occurs when y^c_f is in agreement with y^k_f and the desired agreement is controlled by the value of ϵ_1.

The iterative procedure and discretization technique employed in this paper are similar to that used by [12] and therefore are not repeated here. However, it is important to note that the minimization problem used in this paper is given by Equations (34)–(36) and this is quite different from that used by [14]. Again, we have applied a numerical algorithm that allows less usage of the number of the non-linear constraints so reducing the time taken to obtain convergence. In this paper we use n to denote the reduced number of non-linear constraints, where $n \le m$ and the values considered are $n = m$ and $n = m/2$. Both values of n yield accurate results but $n = m$ takes more computing time. The following results have been found using $m = 40$ and $n = 20$.

3. NUMERICAL RESULTS AND DISCUSSION

In order to illustrate the computational procedure developed in this paper, the numerical calculations for the direct approach were performed on an obstacle of non-dimensional fixed height h_s/h, such that $|h_s/h| \leq 0.4$, and for a given free surface profile with the upstream Froude number greater than unity. These conditions were considered so that the fluid flow over the obstacle always remained supercritical, see Lonyangapuo *et al*. [9]. For most of the examples considered in this paper, all the information about the known non-dimensional free surface height, y_f^k, is found from the direct approach and hence the analytical form of the solid bottom surface is known. This information is useful when discussing the accuracy of the predicted solution. However, the free surface profile for the last example considered in this paper is given arbitrarily and therefore the exact form of the analytical bottom surface is unknown, and we attempt to use the present technique to predict its shape and location.

3.1. Fluid flow over a double hump

First, we apply the minimum kinetic energy method to the first example, namely the case when the bottom surface is a double hump. The geometrical expression for the analytical bottom surface is given by

$$y_b = 0, \qquad x_E \leq x_b < -1 \tag{37}$$

$$y_b = \frac{h_s/h}{2}\left[1 + \cos\left(\frac{4x_b\pi}{L}\right)\right], \qquad -1 \leq x_b \leq (L-1) \tag{38}$$

$$y_b = 0, \qquad (L-1) < x_b \leq x_F \tag{39}$$

By using the direct approach, with $x_F = -3$, $x_F = 5$, $h_s/h = 0.4$, $L = 4.0$, $Fr = 2.0$ and $m = 40$, the numerical non-dimensional free surface height, y_f^k, the non-dimensional fluid speed on the free surface, u_f^k, and the non-dimensional potential function along the free surface, ϕ_f^k, are obtained.

By observing the profile of the given free surface, we conclude that the possible position of the double hump lies in the range $-2.6 \leq x_b \leq 4.6$, and hence $x_1 = -2.6$, $x_2 = 4.6$ and therefore $L^{int} = 7.2$. Here the superscript int is used in order to discriminated between L^{int} and L, where L is the true non-dimensional double hump length. It is important to note that similar results are obtained when the possible position of the double hump is not dependent on observing the free surface profile, i.e. the assumed range is the whole domain $x_E \leq x_b \leq x_F$ so that $x_1 = x_E$, $x_2 = x_F$ and $L^{int} = (x_F - x_E)$. The simple constraints as given by Equation (35) modify to

$$y_b = 0, \qquad -3 \leq x_b < -2.6 \tag{40}$$

$$y_b^{min} \leq y_b \leq y_b^{max}, \qquad -2.6 \leq x_b \leq 4.6 \tag{41}$$

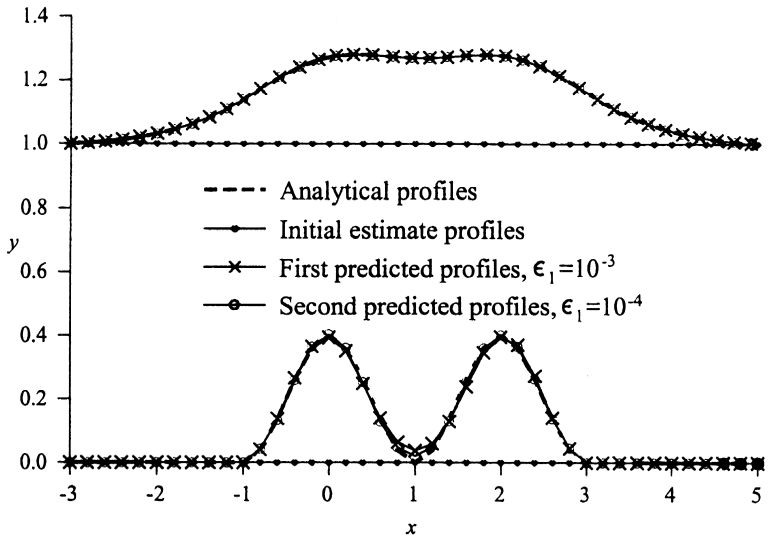

Figure 2. The free and bottom surface profiles for the fluid flow over a double hump when F defined by Equation (34) is minimized, with $\epsilon_1 = 10^{-3}$ and 10^{-4}. The parameter values are $\epsilon_2 = 0$, $L^{\text{int}} = 7.2$, $m = 40$, $n = 20$, $Fr = 2.0$, $y_b^{\min} = -\infty$, $y_b^{\max} = \max(y_f^k)$ and infinity conditions at $x = -3$ and 5, respectively. Also shown for comparison are the analytical bottom surface profile, the numerical free surface profile and the initial estimate profiles for both surfaces.

$$y_b = 0, \qquad 4.6 < x_b \leq 5 \tag{42}$$

where $y_b^{\min} = -\infty$ and $y_b^{\max} = \max(y_f^k)$. The minimal kinetic energy functional, the non-linear constraints and the simple constraints are defined by Equations (34), (36) and (40)–(42), respectively. In order to solve this problem, we need to supply an initial estimate for y_b, denoted by y_b^{int}, and throughout this paper, it is taken to be

$$y_b^{\text{int}} = 0, \qquad -3 \leq x_b \leq 5 \tag{43}$$

where the superscript int denotes the initial value. An iterative procedure is used to solve Equations (34), (36), (40)–(43) $\epsilon_1 = 10^{-3}$ and 10^{-4} for the first and second computed solutions respectively, when $\epsilon_2 = 0$, $L^{\text{int}} = 7.2$. $Fr = 2.0$, $y_b^{\min} = -\infty$, $y_b^{\max} = \max(y_f^k)$, $m = 40$ and $n = 20$. The results obtained are optimal and the predicted bottom surface is in agreement with the analytical result. The optimal values of F, denoted by $F_{\min}$, are -6.9822 and -6.9888, and they compare well with the numerical value obtained from the analytical expression for y_b, namely -6.9894. We see that the value of $F_{\min}$ for both the first and the second computed solutions differ from the numerical value obtained when using the analytical expression for y_b by 7.2×10^{-3} and 6.0×10^{-4} respectively. The profiles of these results are compared with the analytical result, see Figure 2, and it is observed that the predicted bottom

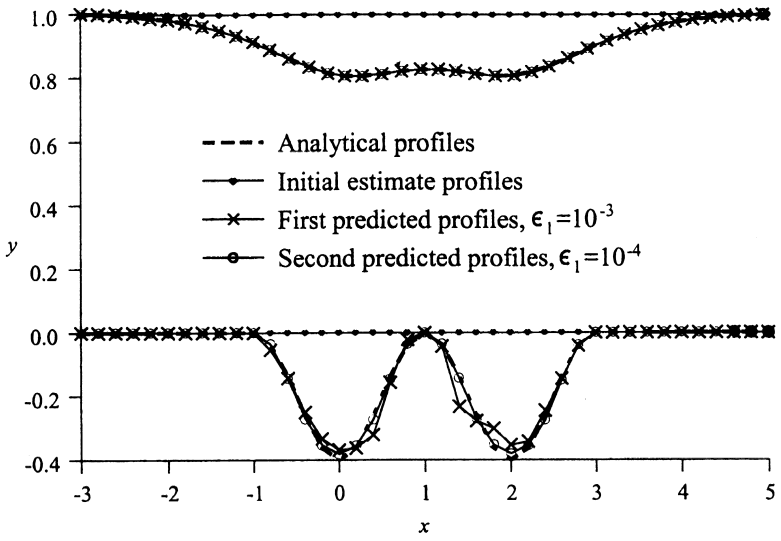

Figure 3. The free and bottom surface profiles for the fluid flow over a double depression when F defined by Equation (34) is minimized, with $\epsilon_1 = 10^{-3}$ and 10^{-4}. The parameter values are $\epsilon_2 = 0$, $L^{\text{int}} = 7.2$, $m = 40$, $n = 20$, $Fr = 2.0$, $y_b^{\min} = -\infty$, $y_b^{\max} = \max(y_f^k)$ and infinity conditions at $x = -3$ and 5, respectively. Also shown for comparison are the analytical bottom surface profile, the numerical free surface profile and the initial estimate profiles for both surfaces.

surface is indistinguishable from the analytical result, especially when $\epsilon_1 = 10^{-4}$. These results are in contrast with those results found in Lonyangapuo *et al.* [14] where it was reported that both the extremal pressure and energy techniques failed to retrieve the required shape and position of the double hump. These results show that the minimal kinetic energy functional is able to identify a complex geometrical bottom surface. However, we need to perform more tests on other complex shapes before any firm conclusions can be established. The following subsection considers the situation when the geometrical bottom surface is a double depression.

3.2. Fluid flow over a double depression

The analytical geometry for the bottom surface of this problem is obtained from Equations (37)–(39) with $h_s/h = -0.4$. The known free surface and the non-dimensional fluid speed on this surface are found by the direct approach. The minimization problem is defined by Equations (34), (36) and (40)–(42), while the initial estimated is given by Equation (43). Again, the value for ϵ_1 is taken to be 10^{-3} and 10^{-4}, and the other parameters values are $\epsilon_2 = 0$, $L^{\text{int}} = 7.2$, $Fr = 2.0$, $y_b^{\min} = -\infty$, $y_b^{\max} = \max(y_f^k)$, $m = 40$ and $n = 20$. The results obtained are optimal and the values of $F_{\min}$ are -6.7772 and -6.778, and they are in good agreement with the analytical value simulated from the analytical expression for y_b, namely -6.7832. In fact they differ from the latter by 6.0×10^{-3} and 4.0×10^{-4} respectively. When the results are graphically compared with the analytical one, they are found to be graphically

indistinguishable, see Figure 3. It is observed from this figure that when $\epsilon_1 = 10^{-3}$ the bottom surface around the region $0 \le x_b \le 2$ is slightly oscillatory, but as ϵ_1 decreases to 10^{-4} the oscillations disappear completely. In fact when $\epsilon_1 = 10^{-4}$, both the predicted and the analytical bottom surfaces are in full agreement. These results show that the minimal kinetic energy functional is able to retrieve both the shape and the position of the double depression occurring on the bottom surface of a channel.

3.3. Fluid flow over a hump in front of a step

We now apply the minimal kinetic energy functional to the case where the bottom surface is a combination of a hump and a step. For simplicity we consider the case where the hump has the same height as the step but it is in front of the step. The non-dimensional geometry of such a bottom is defined as follows:

$$y_b = 0, \qquad x_E \le x_b < -1 \tag{44}$$

$$y_b = \frac{h_s/h}{2}\left[1 + \cos\left(\frac{2x_b\pi}{L_1}\right)\right], \qquad -1 \le x_b \le (L_1 - 1) \tag{45}$$

$$y_b = \frac{h_s/h}{2}\left[1 + \cos\left(\frac{x_b\pi}{L_2}\right)\right], \qquad (L_1 - 1) < x_b \le (L_2 + 1) \tag{46}$$

$$y_b = h_s/h, \qquad (L_2 + 1) < x_b \le x_F \tag{47}$$

where $h_s/h = 0.4$, and $L_1 = 2.0$ and $L_1 = 2.0$ are the non-dimensional lengths of the hump and the step respectively. This problem can still be solved if the non-dimensional hump height and the non-dimensional step height have different values. As in the previous investigations, the known free surface is obtained by the direct approach when $x_E = -3$, $x_F = 5$, $Fr = 2.0$ and $m = 40$, and the assumed position of the double hump is found by observing the profile of the given free surface. For this problem we find the assumed position to lie in the range $-2.4 \le x_b \le 4.4$, and hence $L^{\text{int}} = 6.8$. Thus, the simple constraints now assume the form

$$y_b = 0, \qquad -3 \le x_b < -2.4 \tag{48}$$

$$y_b^{\min} \le y_b \le y_b^{\max}, \qquad -2.4 \le x_b \le 4.4 \tag{49}$$

$$y_b = h_s/h, \qquad 4.4 < x_b \le 5 \tag{50}$$

where $y_b^{\min} = -\infty$ and $y_b^{\max} = \max(y_f^k)$. The minimization problem (34), (36) and (48)–(50) is solved with the initial estimate given by Equation (43) when $\epsilon_1 = 10^{-3}$ and 10^{-4}, and $\epsilon_2 = 0$, $L^{\text{int}} = 6.8$, $Fr = 2.0$, $y_b^{\min} = -\infty$, $y_b^{\max} = \max(y_f^k)$, $m = 40$ and $n = 20$. The results obtained are found to be optimal and the values of $F^{\min}$ are -7.3740 and -7.3781, and they compare well with the analytical value -7.3787. In fact they differ from the latter by 4.7×10^{-3} and 6.0×10^{-3} respectively.

When the profiles of these results are compared with the analytical one, they are found to be in good agreement, and in fact are graphically indistinguishable when $\epsilon_1 = 10^{-4}$, see Figure 4. The results of this problem confirm that the minimal kinetic energy functional is able to retrieve a bottom surface that has a hump in front of a step. In the next subsection we apply the minimal energy functional to the case when the geometrical shape of the bottom surface is highly complex.

3.4. Fluid flow over a depression and a hump in front of a step

This complex geometrical bottom surface is obtained by combining a depression, a hump and a step. From the upstream infinity position until the point where the depression occurs the bottom is of height zero and it is horizontal. After the step the bottom again becomes horizontal and the non-dimensional height is h_s/h. The non-dimensional heights of the depression, the hump and the step can be chosen to be different in magnitude but for the presentation of the results in this paper we set them to be equal. Therefore, the non-dimensional geometrical configuration of the bottom surface can be written as

$$y_b = 0, \qquad x_E \le x_b < -1 \tag{51}$$

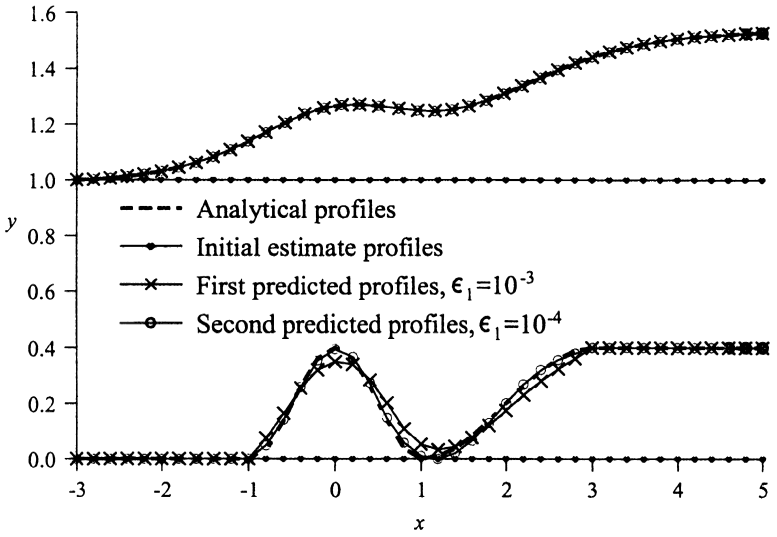

Figure 4. The free and bottom surface profiles for the fluid flow over a hump in front of a step when F defined by Equation (34) is minimized, with $\epsilon_1 = 10^{-3}$ and 10^{-4}. The parameter values are $\epsilon_2 = 0$, $L^{\text{int}} = 6.8$, $m = 40$, $n = 20$, $Fr = 2.0$, $y_b^{\min} = -\infty$, $y_b^{\max} = \max(y_f^k)$ and infinity conditions at $x = -3$ and 5, respectively. Also shown for comparison are the analytical bottom surface profile, the numerical free surface profile and the initial estimate profiles for both surfaces.

$$y_b = \frac{-h_s/h}{2}\left[1+\cos\left(\frac{2x_b\pi}{L_i}\right)\right], \qquad -1 < x_b \le (L_1 - 1) \tag{52}$$

$$y_b = \frac{h_s/h}{2}\left[1+\cos\left(\frac{3x_b\pi}{L_2}\right)\right], \qquad (L_1 - 1) < x_b \le (L_2 + 1) \tag{53}$$

$$y_b = h_s/h, \qquad (L_2 + 1) < x_b \le x_F \tag{54}$$

where $h_s/h = 0.4$, $L_1 = 2.0$ and $L_2 = 3.0$ are the non-dimensional lengths of the depression and the hump in front of a step, respectively. Thus the total non-dimensional analytical length of the complex obstruction is $L = L_1 + L_2 = 5.0$. For this problem we have taken the infinity positions x_E and x_F to be -3 and 7 respectively. Again the known free surface is obtained by the direct approach when $Fr = 2.0$, $|h_s/h| = 0.4$ and $m = 40$. The assumed position of this complex obstruction is found to lie in the range $-2 \le x_b \le 6$, so that $L^{\text{int}} = 8.0$ and therefore the simple constraints become

$$y_b = 0, \qquad -3 \le x_b < -2 \tag{55}$$

$$y_b^{\min} \le y_b \le y_b^{\max}, \qquad -2 \le x_b \le 6 \tag{56}$$

$$y_b = h_s/h, \qquad 6 < x_b \le 7 \tag{57}$$

where, as in the previous investigations, we take $y_b^{\min} = -\infty$ and $y_b^{\max} = \max(y_f^k)$. As in the previous cases, F is given by Equation (34) while the non-linear constraints and the modified simple constraints are given by Equations (36) and (55)–(57), whilst the initial estimate for y_b is given by

$$y_b^{\text{int}} = 0, \qquad -3 \le x \le 7 \tag{58}$$

The computed solutions are obtained with $\epsilon_1 = 10^{-3}$ and 10^{-4}, and the parameter values are $\epsilon_2 = 0$, $L^{\text{int}} = 8.0$, $Fr = 2.0$, $y_b^{\min} = -\infty$, $y_b^{\max} = \max(y_f^k)$, $m = 40$ and $n = 20$. The results obtained are optimal and the predicted profiles for both surfaces are in agreement with the analytical solution, see Figure 5. The optimal values of $F_{\min}$ are -5.3378 and -5.3464, and both compare very well with the analytical value -5.3473. We can see that the values of $F_{\min}$ for both the first and the second computed solutions differ from the latter by 9.5×10^{-3} and 9.0×10^{-4} respectively. These results show that the minimal kinetic energy is able to retrieve a highly complex geometrical bottom surface. These successful results mean that we can now generalize that the minimal kinetic energy functional is able to locate both the position and the shape of any unknown bottom surface of a channel. This conclusion has been arrived at after the success of this technique when applied to the problems presented in Sections 3.1–3.4.

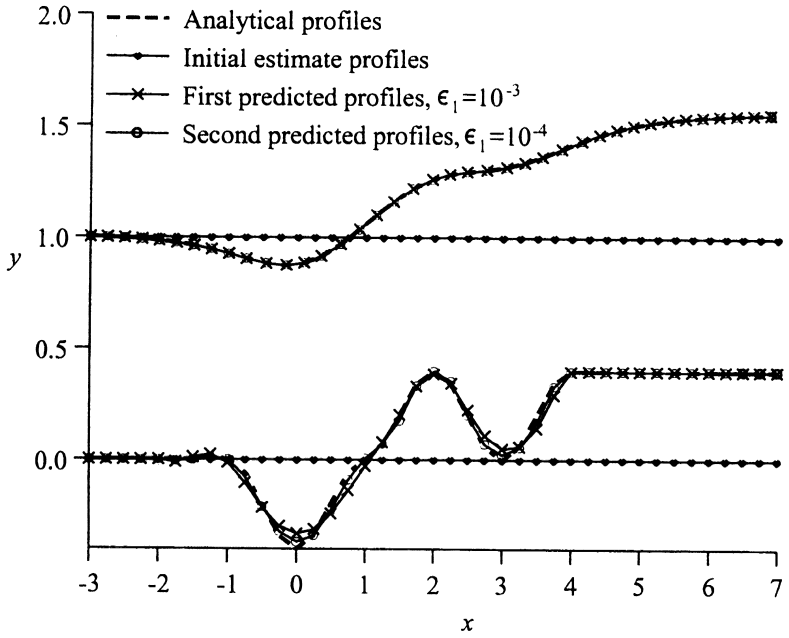

Figure 5. The free and bottom surface profiles for the fluid flow over both a depression and a hump in front of a step when F defined by Equation (34) is minimized, with $\epsilon_1 = 10^{-3}$ and 10^{-4}. The parameter values are $\epsilon_2 = 0$, $L^{\text{int}} = 8.0$, $m = 40$, $n = 20$, $Fr = 2.0$, $y_{\text{b}}^{\min} = -\infty$, $y_{\text{b}}^{\max} = \max(y_{\text{f}}^{\text{k}})$ and infinity conditions at $x = -3$ and 5, respectively. Also shown for comparison are the analytical bottom surface, profile, the numerical free surface profile and the initial estimate profiles for both surfaces.

3.5. Free surface profile from $y = \tanh(x)$

3.5.1. The domain of the fluid flow is $-5 \le x \le 7$. We now apply the minimal kinetic energy functional to the case where the known non-dimensional free surface height, y_{f}^{k}, is expressed by a tanh function. Suppose the tanh function is given as follows:

$$y_{\text{f}}^{\text{k}} = c_1 + c_2[\tanh(x_{\text{f}})], \quad x_E \le x_{\text{f}} \le x_F \tag{59}$$

where c_1 and c_2 are two arbitrary constants, and as usual x_E and x_F denote the far upstream and downstream infinity positions respectively. In order to demonstrate the results obtained for this section we let c_1 and c_2 take the values 1.275885 and 0.275885 respectively, and these values set the non-dimensional free surface height far upstream and downstream to have values 1.0 and 1.35177 respectively. The values of x_E and x_F are found to lie in the ranges $-10 \le x_E \le -3$ and $3 \le x_F \le 10$ respectively. In order to show the consistency of the results obtained when x_E and x_F take on different values we consider two cases. First, we solve the problem when the values of x_E and x_F are taken to be -5 and 7, respectively, and then when

the values are -3 and 3. The functional F is given by Equation (34), while the non-linear constraints as given by Equation (36), can be written as

$$(y_{fj}^{k} - \epsilon_1) \leq y_{fj}^{c} \leq (y_{fj}^{k} + \epsilon_2), \quad j = 1, 2, \ldots, n \tag{60}$$

where y_f^k is given by Equation (59). However, the simple constraints are not immediately available, since the non-dimensional height of the bottom surface at the far downstream position is not given directly. At the far downstream infinity position on the free surface the non-dimensional height is a constant and the fluid flow is horizontal. Therefore we can use the one-dimensional theory, where at the far downstream infinity position $x = x_M = x_F$ the non-dimensional height of the bottom surface, $h_s/h = y_b(x_F)$, may be obtained from

$$Fr^2 + 2 = \frac{Fr^2}{(y_M - h_s/h)^2} + 2y_M \tag{61}$$

which is Equation (3) with y_f and U_f/U_∞ replaced by h_s and $h/(Y_M - h_s)$ respectively. By putting $Fr = 2.0$ and $y_M = 1.35177$ into Equation (61), we find the value of h_s/h to be approximately equal to 0.35. Since the given non-dimensional free surface height at the far upstream infinity is unity, we conclude that the corresponding non-dimensional height for the bottom surface is zero. Thus we find that the far upstream and downstream infinity positions for the non-dimensional bottom surface are $(-5, 0)$ and (7, 0.35) respectively. By plotting the profile of the given free surface we see that the free surface is horizontal in the regions $-5 \leq x < -4.5$ and $6.5 < x \leq 7$. From these observations we conclude that the solid obstacle lies in the region $-4.5 \leq x \leq 6.5$ and hence the estimated non-dimensional length of the obstacle is $L^{int} = 11.0$. Therefore the simple constraints given by Equation (35) now take the form

$$y_b = 0, \qquad -5 \leq x_b < -4.5 \tag{62}$$

$$y_b^{min} \leq y_b \leq y_b^{max}, \qquad -4.5 \leq x_b \leq 6.5 \tag{63}$$

$$y_b = h_s/h, \qquad 6.5 < x_b \leq 7 \tag{64}$$

where $h_s/h = 0.35$, $y_b^{min} = -\infty$ and $y_b^{max} = \max(y_f^k)$.

The minimization problem is defined by Equations (34), (36) and (62)–(64) while the initial estimate is taken to be

$$y_b^{int} = 0, \qquad -5 \leq x_b \leq 7 \tag{65}$$

As in the previous investigations F_{min} is solved by taking $\epsilon_1 = 10^{-3}$ and 10^{-4} for the first and second computed solutions respectively, while the parameter values are $\epsilon_2 = 0$, $L^{int} = 11.0$, $Fr = 2.0$, $y_b^{min} = -\infty$, $y_b^{max} = \max(y_f^k)$, $m = 40$ and $n = 20$. The results obtained for both $\epsilon_1 = 10^{-3}$ and 10^{-4} are optimal and in fact they are very similar with the value of F_{min} being -3.2318. Hence, we conclude that the required shape of the bottom surface has been identified. On comparing the computed free surface profiles with the given one, we find that they are graphically indistinguishable, see Figure 6. In order to establish that the predicted bottom surface is the required one we use the predicted values of the non-dimensional height

of the bottom surface, y_b^{opt}, and the angle that this surface makes with the horizontal, β, in the algorithm for the direct problem, see Lonyangapuo *et al.* [9]. When this is undertaken we find that the predicted free surface is in agreement with the given free surface. Therefore we conclude that the minimal kinetic energy is robust enough to retrieve an unknown bottom surface whose free surface is given *a priori*.

3.5.2. The domain of the fluid flow is $-3 \le x \le 3$. In order to conclude the results of this problem it is appropriate to reduce the domain of the free surface fluid flow and then compare the predicted shapes of the bottom with those shown in Figure 6. Let the infinity positions x_E and x_F take the values -3 and 3, respectively. The given free surface is that given by Equation (59), and observing the profile of this surface we conclude that the non-horizontal part of the free surface lies in the range $-2.5 \le x \le 2.5$, so that $L^{int} = 5.0$. Thus the simple constraints become

$$y_b = 0, \qquad -3 \le x_b < -2.5 \tag{66}$$

$$y_b^{min} \le y_b \le y_b^{max}, \qquad -2.5 \le x_b \le 2.5 \tag{67}$$

$$y_b = h_s/h, \qquad 2.5 < x_b \le 3 \tag{68}$$

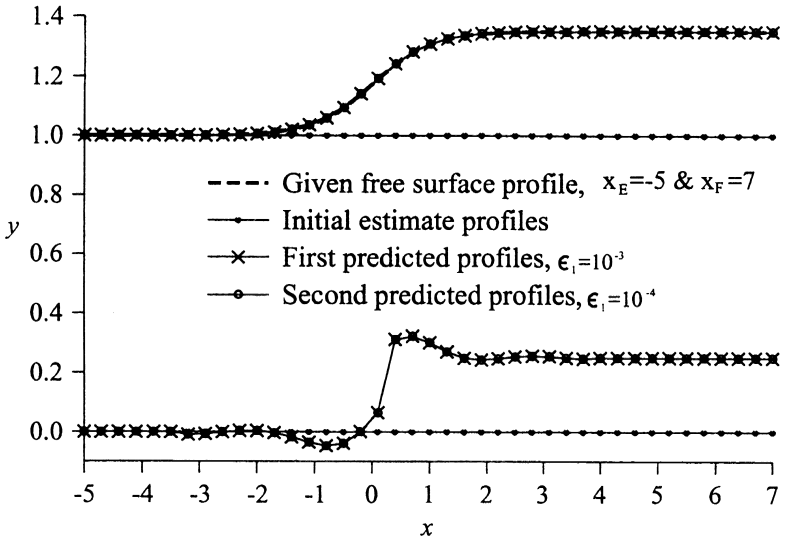

Figure 6. The free and bottom surface profiles for the fluid flow over an unknown solid obstacle when F defined by Equation (34) is minimized, with $\epsilon_1 = 10^{-3}$ and 10^{-4}. The parameter values are $\epsilon_2 = 0$, $L^{int} = 11.0$, $m = 40$, $n = 20$, $Fr = 2.0$, $y_b^{min} = -\infty$, $y_b^{max} = \max(y_f^k)$ and infinity conditions at $x = -5$ and $x = 7$, respectively. Also shown for comparison is the profile of the given free surface generated from Equation (59) and the initial estimate profiles for both surfaces.

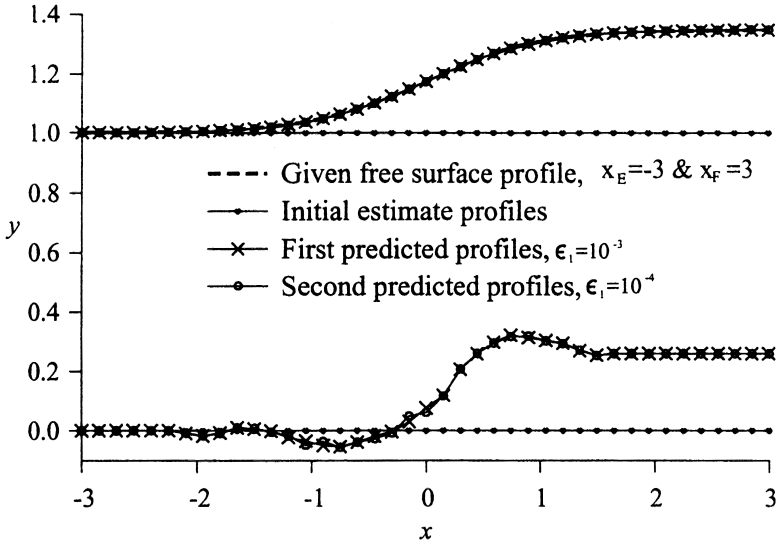

Figure 7. The free and bottom surface profiles for the fluid flow over an unknown solid obstacle when F defined by Equation (34) is minimized, with $\epsilon_1 = 10^{-3}$ and 10^{-4}. The parameter values are $\epsilon_2 = 0$, $L^{\text{int}} = 5.0$, $m = 40$, $n = 20$, $Fr = 2.0$, $y_b^{\min} = -\infty$, $y_b^{\max} = \max(y_f^k)$ and infinity conditions at $x = -3$ and $x = 3$, respectively. Also shown for comparison is the profile of the given free surface generated from Equation (59) and the initial estimate profiles for both surfaces.

where $h_s/h = 0.35$, $y_b^{\min} = -\infty$ and $y_b^{\max} = \max(y_f^k)$. The minimization problem is defined by Equations (34), (36) and (66)–(68) respectively, while the initial estimate, y_b^{int}, is expressed as

$$y_b^{\text{int}} = 0, \qquad -3 \le x_b \le 3 \tag{69}$$

As usual, the computed solutions are found with $\epsilon_1 = 10^{-3}$ and 10^{-4}, and the other parameter values $\epsilon_2 = 0$, $L^{\text{int}} = 5.0$, $Fr = 2.0$, $y_b^{\min} = -\infty$, $y_b^{\max} = \max(y_f^k)$, $m = 40$ and $n = 20$. The results obtained are also optimal and the predicted free surface profiles are in agreement with the analytical profile, see Figure 7. The predicted bottom surface profiles for both solutions are also in good agreement and are similar to those shown in Figure 6. Therefore we conclude that the required shape and position has been identified. The optimal values of $F_{\min}$ are -9.1919 and -9.1922, and they differ from each other by about 3.0×10^{-4}.

4. CONCLUSIONS

We have used the minimal kinetic energy functional to investigate the position and shape of the bottom surface of a channel in a two-dimensional, steady, inviscid, incompressible and irrotational fluid flow under the effect of gravity. This technique has been applied to retrieving

the simple geometrical bottom surfaces which were investigated in Lonyangapuo *et al.* [10–14]. We have found that the minimal kinetic energy is sufficiently robust in identifying these bottom surfaces, and unlike the previous techniques we only solve for the minima and not the maxima of the functional. Next, we applied this technique to retrieving the shapes and positions of both a double hump and a double depression. We note that these shapes could not be recovered by using the extremal pressure and energy functionals, see Lonyangapuo *et al.* [12–14]. However, we have found that the minimal kinetic energy functional retrieves all these bottom surfaces and the optimal values of $F_{\min}$ are in very good agreement with their analytical values.

On extending the technique to even more complex geometrical bottom surfaces, we have found that the present technique is able to retrieve all those that we have investigated. For example, we have solved the fluid flow over a hump in front of a step and the fluid flow over both a depression and a hump in front of a step. The results obtained are excellent for each problem, and in fact the computed profiles for both surfaces are graphically indistinguishable from the analytical results. This technique has also been extended to solving inverse free surface fluid flows when the free surface profile is given analytically but the form of the analytical bottom surface is not known *a priori*. As an example of such a case we investigated for the position and shape of the unknown bottom surface when the free surface is given by the function $y = \tanh(x)$. The results obtained are extremely accurate and as a validation we used the optimal values of y_b in the algorithm for the direct approach, see Lonyangapuo *et al.* [9]. The predicted free surface was found to agree very well with the analytical free surface. In conclusion, we see that the minimal kinetic energy functional is able to recover any bottom surface provided that the free surface is given *a priori*.

Clearly real problems involve the flow of viscous fluids in complex three-dimensional geometrical situations over a range of upstream Froude numbers. However, the theory in the present paper has been restricted to flows in which the upstream Froude number is supercritical, since in such problems there is not likely to be upstream waves. Any modification of the present analysis to include viscosity is not possible since this would require the solution of the Navier–Stokes equation as opposed to the Laplace equation. Although, as the fluids being studied relate to those with small coefficients of viscosity and hence the corresponding flows are at high Reynolds number, it is likely that the real physical situation can be reasonably modelled by the Laplace equation, but any measurements from field data would be those modified by viscosity. This can be viewed as the potential solution combined with some form of smooth noisy boundary data, and as the present approach indicates that the problem is stable for such situations then we would expect the numerical identification of the bottom surface to the reasonable close to the true situation. Finally, the three-dimensional aspects relating to the direct problem need much further study before any possible extension to the inverse situation is even contemplated, especially as the Riemann–Hibert technique used in the present work, and in much of the research in direct problems, is only applicable to two-dimensional fluid flows.

ACKNOWLEDGMENTS

We wish to acknowledge the financial support from the UK Commonwealth Scholarship Commission for J.K. Lonyangapuo.

REFERENCES

1. Forbes LK, Schwartz LW. Free surface flow over a semicircular obstruction. *Journal of Fluid Mechanics* 1982; **114**: 299–314.
2. Boutrous YZ, El-Malek M. Hilbert's method for numerical solution of flow from a uniform channel over irregular bottom topographies. *Computer Methods in Applied Mechanics and Engineering* 1987; **65**: 215–227.
3. King AC, Bloor MIG. Free surface flow for a stream obstruction by an arbitrary bed topography. *Quarterly Journal in Mechanics and Applied Mathemathics* 1990; **43**: 87–106.
4. Wen X, Wu C. Boundary integral equation inverse method for free surface gravity flows. *Sciential Sinica*, *Series A* 1987; **30**: 992–1008.
5. Wen X, Ingham DB. Flow induced by a submerged source or sink in a three-layer fluid. *Computers and Fluids* 1992; **21**: 133–144.
6. Muskhelishvili NI. *Singular Integral Equations*. P. Noordhoff: Groningen, 1953 (translated and edited by JRM Radock).
7. Wen X, Manik K, Ingham DB. A boundary integral technique for free surface flows under gravity. In *Proceedings of Hydraulic Engineering Software*, vol. VI, Blain WR (ed.). Computational Mechanics Publications: Southampton, 1996; 437–446.
8. Wen X, Ingham DB, Widodo B. The free surface fluid flow over a step of an arbitrary shape in a channel. In *Engineering Analysis with Boundary Elements*, vol. 9, Brebbia CA, Tanaka M, Aliabadi MH, Cheng A (eds), 1997; 299–308.
9. Lonyangapuo JK, Elliott L, Ingham DB, Wen X. The critical height of a step in a channel for a wave-free potential free surface flow. In *Proceedings of the First UK Conference on Boundary Integral Methods*, Elliott L, Ingham DB, Lesnic D (eds). Leeds University Press: Leeds, 1997; 202–212.
10. Lonyangapuo JK, Elliott L, Ingham DB, Wen X. Identification of the shape of the bottom surface of a channel from a given free surface profile. In *Proceedings of EUROBEM*, Brebbia CA (ed.). Computational Mechanics Publications: Southampton, 1998; 81–90.
11. Lonyangapuo JK, Elliott L, Ingham DB, Wen X. Retrieval of the shape of the bottom surface of a channel when the free surface profile is given. *Engineering Analysis with Boundary Elements* 1999; **23**: 457–470.
12. Lonyangapuo JK, Elliott L, Ingham DB, Wen X. A boundary integral technique for solving for an unknown bottom surface given a free surface fluid flow. In *International Series on Advances in Boundary Elements*, vol. 6, *Boundary Elements XXI*, Brebbia CA, Power H (eds). Oxford University Press: Oxford, 1999; 365–374.
13. Lonyangapuo JK, Elliott L, Ingham DB, Wen X. Flow in channels over rigid obstacles of unknown shape. In *Proceedings of the Second UK Conference on Boundary Integral Methods*, Wrobel LC, Chandler-Wilde S (eds). Brunel University Press, 1999; 165–176.
14. Lonyangapuo JK, Elliott L, Ingham DB, Wen X. Use of an extremal functional in solving for an unknown bottom surface given a free surface profile. *Engineering Analysis with Boundary Elements* 2000; **24**: 17–30.
15. Lamb H. *Hydrodynamics* (6th edn). University Press: Cambridge, 1932.
16. Ramsey AS. *A Treatise on Hydromechanics*, *Part III*, *Hydrodynamics*. G. Bell and Sons: London, 1920.
17. Gill PE, Murray W, Wright MH. *Practical Optimization*. Academic Press: London and New York, 1981.

